Bull. Mater. Sci., Vol. 33, No. 2, April 2010, pp. 169–178. © Indian Academy of Sciences.

Charge-order driven multiferroic and magneto-dielectric properties of rare earth manganates

CLAUDY RAYAN SERRAO[1,2,*], JYOTI RANJAN SAHU[1] and ANIRBAN GHOSH[1,2]

[1]Chemistry and Physics of Materials Unit, Jawaharlal Nehru Centre for Advanced Scientific Research, Bangalore 560 064, India

[2]Materials Research Centre, Indian Institute of Science, Bangalore 560 012, India

MS received 23 January 2009

Abstract. **Charge-order driven magnetic ferroelectricity is shown to occur in several rare earth manganates of the general formula, $Ln_{1-x}A_xMnO_3$ (Ln = rare earth, A = alkaline earth). Charge-ordered manganates exhibit dielectric constant anomalies around the charge-ordering or the antiferromagnetic transition temperature. Magnetic fields have a marked effect on the dielectric properties of these compounds, indicating the presence of coupling between the magnetic and electrical order parameters. Magneto-dielectric properties are retained in small particles of the manganates. The observation of magneto-ferroelectricity in these manganates is in accordance with theoretical predictions.**

Keywords. **Multiferroics; magnetoelectric effect; magnetocapacitance; rare earth manganates.**

1. Introduction

Materials which exhibit both magnetic and electrical ordering are attracting great interest in the last few years, partly because of their technological potential. Besides a range of possible device applications, the science of these materials is truly fascinating (Prellier *et al* 2005; Eerenstein *et al* 2006; Cheong and Mostovoy 2007; Ramesh and Spaldin 2007; Rao and Serrao 2007). Multiferroics are materials in which ferromagnetism, ferroelectricity and ferroelasticity occur in the same phase. This implies that they possess spontaneous magnetization which can be reoriented by an applied magnetic field, a spontaneous polarization which can be reoriented by an applied electric field and a spontaneous deformation which can be reoriented by an applied stress. It is, however, customary to exclude ferroelasticity and only consider magnetic and ferroelectric characteristics. Multiferroics possess neither spatial inversion symmetry nor time-reversal symmetry.

It is generally difficult to find materials that are magnetic as well as ferroelectric, since conventional ferroelectricity occurs when the metal ions have empty *d*-orbitals. Magnetism, on the other hand, occurs in materials containing cations with partially filled *d*-orbitals. Magnetoelectrics are simultaneously ferromagnetic and ferroelectric in the same phase, with coupling between the two orders. Magnetoelectric coupling describes the influence of a magnetic (electric) field on the polarization (magnetization) of a material. Magnetoelectric coupling can exist independent of the nature of the magnetic and electrical order parameters. It is an independent phenomenon which may not necessarily arise in materials that are both magnetically and electrically polarizable. Since coexistence of magnetic and ferroelectric ordering is not favoured, materials with such properties arising from alternative mechanisms are being sought in recent years.

One of these mechanisms is tilting of MnO_5 trigonal bypyramids giving rise to ferroelectricity as in the case of $YMnO_3$ (Van Aken *et al* 2004). Bismuth compounds such as $BiMnO_3$ and $BiFeO_3$ exhibit ferroelectric properties because of the stereochemical activity of the Bi lone pair (Seshadri and Hill 2001), while in $TbMnO_3$, spiral magnetic ordering is the source of ferroelectricity (Kimura *et al* 2003). One of the new mechanisms is to induce ferroelectricity and magnetoelectric effects in oxide materials is cation charge-ordering as in the case of some of the rare earth ferrites of the type, $LnFe_2O_4$ (Ln = rare earth) (Serrao *et al* 2007). In this article we shall discuss multiferroicity and magnetoelectric effects in rare earth manganates induced by charge-ordering as theoretically predicted by Efremov *et al* (2004).

1.1 *Charge-ordering in rare earth manganates*

Rare earth manganates of the type, $Ln_{(1-x)}A_xMnO_3$ (Ln = rare earth ion, and A = alkaline earth ion), which crystallize in the perovskite structure were investigated several years ago by Wollan and Koehler (1955). However, it was the discovery of colossal magneto resistance (CMR) that has

*Author for correspondence (claudy@jncasr.ac.in)

attracted recent attention to these materials (Rao and Raveau 1998; Salamon and Jaime 2001; Tokura 2006). In the parent $LaMnO_3$, the Mn ions exist in a 3+ state, while $La_{(1-x)}Ca_xMnO_3$ contains both Mn^{3+} and Mn^{4+} ions. The phase diagram of this system reveals a large number of phases with different electronic properties. $LaMnO_3$ exhibits a spin order of an A-type antiferromagnet. This is accompanied by the orbital order which is coupled to the lattice distortion due to the Jahn–Teller (JT) effect. The JT distortion looses long-range order around 750 K. At low temperatures, the combination of orbital ordering and JT distortion leads to a ferromagnetic (FM) exchange interaction between the spins in the *ab* plane, and a antiferromagnetic (AFM) interaction between the planes, resulting in an *A*-type AFM arrangement.

Doping the rare earth manganates with alkaline earth ions such as Ca^{2+} and Sr^{2+} gives rise to charge ordering wherein the +3 and +4 charges of the Mn ions are arranged in a periodic fashion (figure 1) (Rao 2000). The charge-ordered state occurs commonly in the manganates containing small Ln and A ions, and disappears at high temperatures. For example, in $Pr_{0.6}Ca_{0.4}MnO_3$, charge ordering occurs below 230 K (T_{CO}). It shows AFM order below 170 K, where both antiferromagnetism and charge order coexist (figure 2) (Lees *et al* 1995; Tomioka *et al* 1996). At low temperatures, this manganate is an insulator. Application of magnetic fields destroys the charge-ordered state. In contrast, $La_{0.7}Ca_{0.3}MnO_3$ does not show charge ordering, although it enters a FM metallic phase below a Curie temperature of 230 K, showing a paramagnetic (PM) insulating behaviour above this temperature. This is a typical manganate composition exhibiting colossal magnetoresistance (Rao and Raveau 1998). In the Sr-based $La_{0.7}Sr_{0.3}MnO_3$, the high temperature PM phase is metallic. Note that the average radius of the *A*-site cations, $\langle r_A \rangle$, is larger in these two lanthanum manganates than in $Pr_{0.7}Ca_{0.3}MnO_3$. An important aspect of the doped manganates is that, when the size of the *A*-site cation (or the e_g bandwidth) is large enough, electrons of the Mn^{3+} hop to Mn^{4+} by the double-exchange (DE) mechanism (Rao and Raveau 1998; Salamon and Jaime 2001; Tokura 2006). The DE mechanism plays a crucial role in the occurrence of metallicity and ferromagnetism in these materials. The phenomenon of CMR is explained by invoking the DE mechanism along with certain competing interactions involving phonons. Charge ordering has an effect opposite to that of DE, since it localizes electrons creating an AFM insulating state.

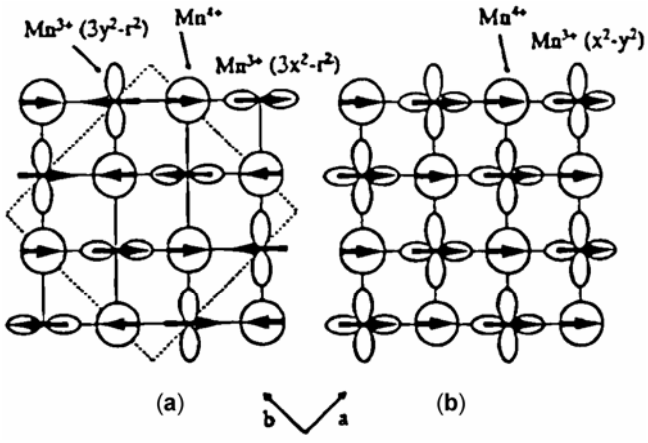

Figure 1. Ordering of charge, spin and orbital in doped manganates: (**a**) CE-type order, the dashed line shows the unit cell and (**b**) *A*-type order. In both figures, circles correspond to Mn^{4+} (Rao 2000).

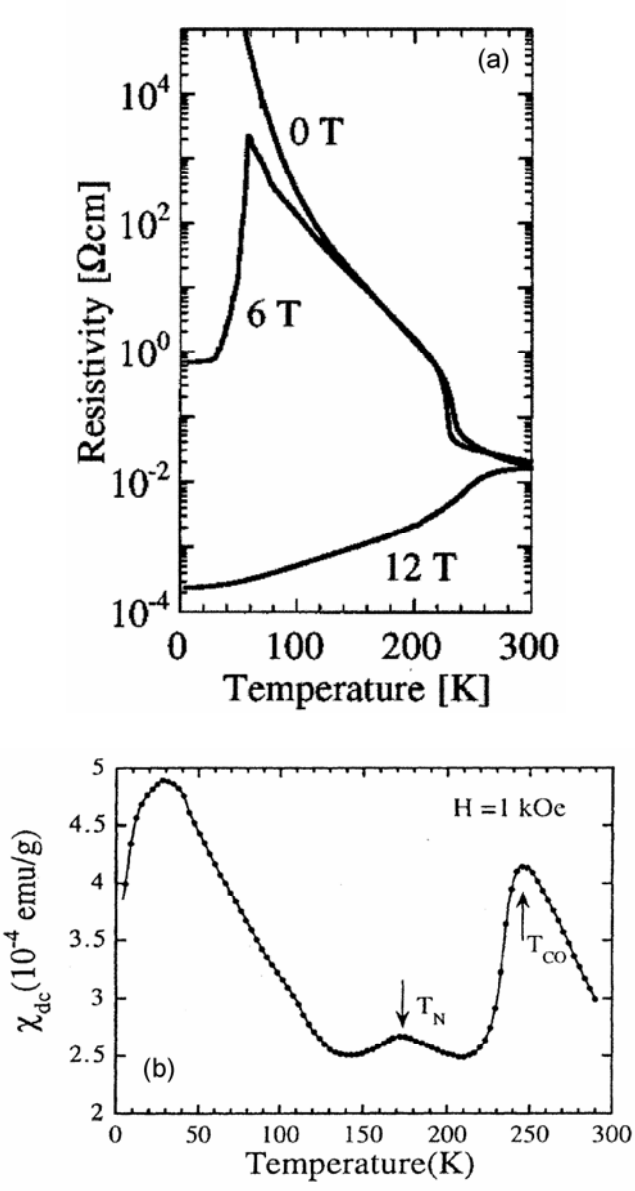

Figure 2. Temperature variation of (**a**) resistivity and (**b**) magnetic susceptibility of $Pr_{0.6}Ca_{0.4}MnO_3$. The increase in magnetization at low temperatures (<100 K) is due to electronic phase separation (Lees *et al* 1995; Tomioka *et al* 1996).

Half-doped rare earth manganates show many interesting types of electronic order. For example, $Nd_{0.5}Sr_{0.5}MnO_3$, which is a FM metal around room temperature undergoes a transition to a charge-ordered AFM insulator state around 150 K (figure 3) (Kuwahara *et al* 1995). At low temperatures, the charge-ordered state is associated with a CE-type AFM order (figure 1), orbital order as well as a pattern due to JT distortions. The magnetic order consists of *ab* planes stacked along the *c*-axis with an AFM coupling between spins on neighbouring planes and is different from the *A*-type order. Note that there is no charge ordering in an *A*-type antiferromagnet unlike in a CE-type antiferromagnet. Generally, orbital and spin orders which are not accompanied by charge order show *A*-type antiferromagnetism.

The presence of charge order and orbital order is readily found experimentally by a study of the structures of the manganates (figure 4) (Vogt *et al* 1996; Woodward *et al* 1999). For example, the charge-ordered structure of $Nd_{0.5}Sr_{0.5}MnO_3$ consists of distorted oxygen octahedra with zigzag chains with alternate long and short Mn–O bonds. In terms of the chemistry, the mean *A*-site cation radius $\langle r_A \rangle$ is expected to play an important role. This arises from the fact that the bandwidth of the e_g electrons of Mn ions is affected by the size of the *A*-site cation. That is, increasing $\langle r_A \rangle$ is equivalent to increasing the hydrostatic pressure, which increases the Mn–O–Mn bond angle and consequently the bandwidth. Detailed studies of the effect of $\langle r_A \rangle$ on the electronic order have been reported in the literature (Rao 2000). Manganates with very large $\langle r_A \rangle$ tend to be FM and metallic, with the Curie temperature T_C increasing with $\langle r_A \rangle$. Charge ordering is also strongly affected by $\langle r_A \rangle$, with a smaller $\langle r_A \rangle$ stabilizing the charge-ordered state at low temperatures. It is evident that the tuning of $\langle r_A \rangle$ provides an important means of controlling the electronic order of the manganate. Furthermore, charge ordering can be destroyed to obtain a FM metallic state (Rao 2000) by applying magnetic fields (figures 3 and 5) (Kuwahara *et al* 1995) or electric fields (figure 6) (Rao *et al* 2000). Chemical doping (e.g. by ruthenium) can also produce similar effects (Rao 2000). Two types of charge ordering can be distinguished in rare earth manganates. These are site-centred charge ordering (SCO) and bond-centred charge ordering (BCO) which occur around $x = 0{\cdot}5$ and $x = 0{\cdot}4$ compositions. The two types of charge order are depicted in figure 7 (Efremov *et al* 2004).

1.2 *Electronic phase separation in rare earth manganates*

There is considerable experimental evidence to indicate that several correlated oxides are electronically inhomogeneous (figure 8). This is manifested best in the rare earth manganates (Dagotto 2005; Shenoy *et al* 2006; Shenoy and Rao 2008). Materials with chemical inhomogeneity consist of different spatial regions with different electronic orders. This phenomenon has come to be known as electronic phase separation. The different regions can be static or dynamic and can be tuned by the application of external stimuli like a magnetic field or an electrical field. Moreover, the size scale of these inhomogeneities can vary from nanometers to as large as micrometers.

Investigations by several experimental probes show the presence of electronic inhomogeneities. When the length-scale of the inhomogeneities is large (a few hundred nanometers), structural and magnetic information from the X-ray and neutron diffraction patterns show distinct signatures. Local probes such as NMR and Mössbauer spectroscopies are used to probe inhomogeneities at a smaller length-scale. Magnetization and transport measurements also indicate the presence of inhomogeneities.

Wollan and Koehler (1955) showed many years ago the presence of electronic inhomogeneities, by the observation of both FM and AFM peaks in the magnetic structure of $La_{1-x}Ca_xMnO_3$ by neutron scattering. Neutron diffraction studies of Woodward *et al* (1998) on $Nd_{0.5}Sr_{0.5}MnO_3$ shows that this material first becomes FM at 250 K, partially transforms to an *A*-type AFM phase around 220 K, followed by a transformation of a substantial fraction to a CE-type AFM phase at 150 K. The CE-type

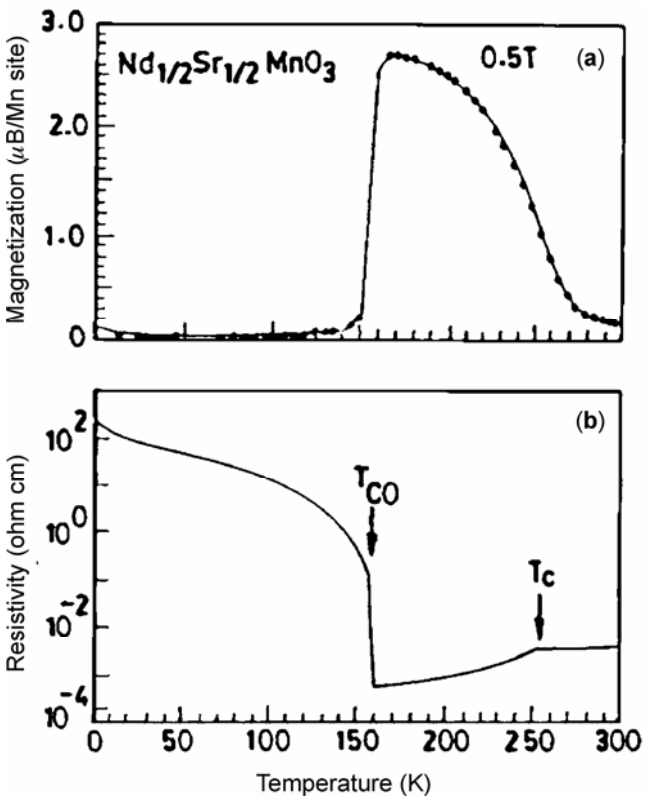

Figure 3. Temperature variation of (**a**) the magnetization and (**b**) the resistivity of $Nd_{0.5}Sr_{0.5}MnO_3$ (Kuwahara *et al* 1995).

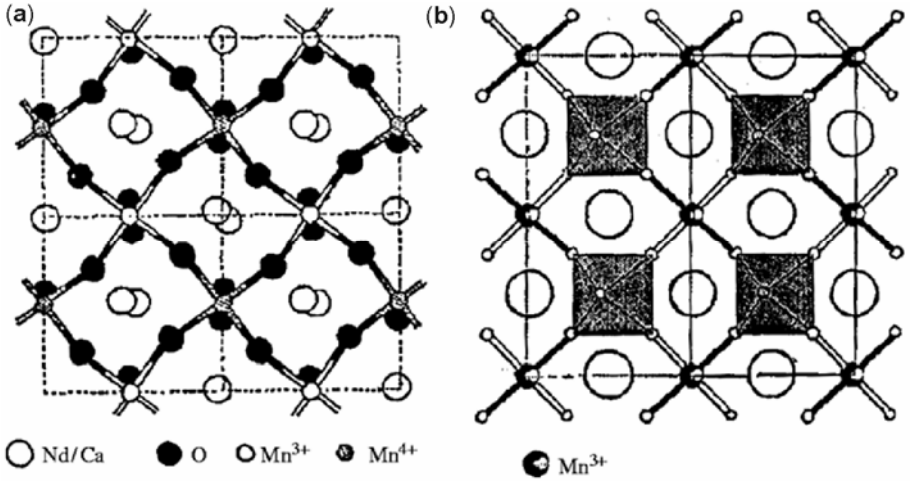

Figure 4. (**a**) Structure of charge-ordered $Nd_{0.5}Sr_{0.5}MnO_3$ in the *ab* plane at 10 K. Mn^{4+} ions are located at (1/2, 0, 0) and Mn^{3+} are located at (0, 1/2, 0). The structure contains zigzag chains with alternate long and short Mn–O bonds. (**b**) The same structure as given in (**a**), shown in polyhedral representation (Vogt *et al* 1996; Woodward *et al* 1999).

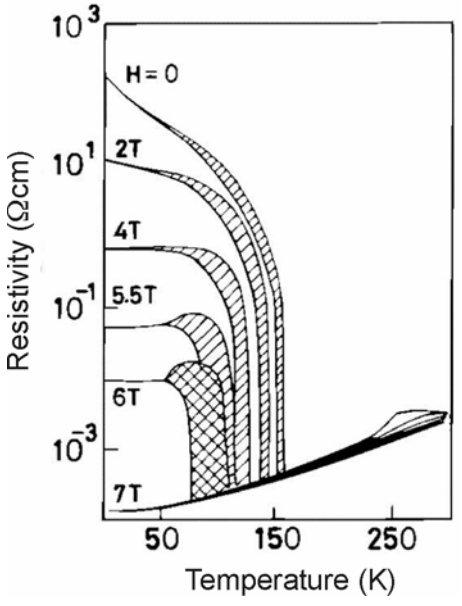

Figure 5. Effect of magnetic fields on the charge ordering transition of $Nd_{0.5}Sr_{0.5}MnO_3$ (Kuwahara *et al* 1995).

AFM phase has a simultaneous ordering of charge, spins and orbitals in a complex spatial arrangement. The three phases coexist at low temperatures. The size scale of the inhomogeneities is atleast in the mesoscopic range (a few hundred nanometers or more), since they are large enough to produce well-defined reflections in neutron and X-ray diffraction patterns. The variation of the volume fraction of the three phases with temperature is shown in figure 9 (Woodward *et al* 1999). This phase diagram has an unusual feature with the three phases existing at the 150 K transition and below. The phase separation observed here is non-trivial in contrast to a situation where the sample is not phase-pure containing multiple phases that are both structurally and chemically distinct. Another interesting example of phase separation is in $Pr_{0.7}Ca_{0.3}MnO_3$, which shows the presence of two distinct phases below the charge-ordering transition at 80 K. A charge-ordered AFM phase and a charge-delocalized phase have been observed by neutron diffraction.

Signatures of electronic inhomogeneities may be inferred from magnetic and electron transport measurements as well. Thus, in $(La_{1-x}Ln_x)_{0.7}Ca_{0.3}MnO_3$, where Ln = Nd, Gd or Y, the lanthanide element was varied to control the average A-site cation radius $\langle r_A \rangle$ (Sudheendra and Rao 2003). In the case of the La compound ($x = 0{\cdot}0$) with the largest value of $\langle r_A \rangle$, a clear FM transition with a saturation magnetization of 3 μ_B is observed up to a critical Nd doping of $x \leq x_c \approx 0{\cdot}5$ (figure 10a) (Sudheendra and Rao 2003). At higher values of Nd doping ($x > x_c$), there is a monotonic increase of the magnetization with decrease in temperature, although the magnetization does not attain the maximum value of 3 μ_B. Reducing the value of $\langle r_A \rangle$ by Gd or Y (smallest value of $\langle r_A \rangle$) substitution, decreases the x_c, i.e. the critical doping value x above which the sharp FM transition vanishes, reduces with the mean A-site cation radius $\langle r_A \rangle$. Moreover, the FM transition temperature, T_c, for $x < x_c$ increases with $\langle r_A \rangle$ as expected. The reduction of the saturation magnetization at $x \geq x_c$ is a signature of electronic and magnetic inhomogeneities induced by the A-site cation disorder. Transport measurements also show the signature of electronic inhomogeneities (figure 10b) (Sudheendra and Rao 2003).

All the $(La_{1-x}Ln_x)_{0.7}Ca_{0.3}MnO_3$ compositions with Ln = Nd, Gd and Y exhibit a metal–insulator transition when $x < x_c$. The insulator–metal transition temperature de-

creases linearly on doping and increases nearly linearly with $\langle r_A \rangle$. Electronic phase separation in such manganates generally occurs when $\langle r_A \rangle$ is relatively small (< 1·18 Å) and is favoured by size disorder arising from the size mismatch between the A-site cations. This disorder is quantified by the parameter $\sigma^2 = \Sigma_i x_i r_i^2 - \langle r_A \rangle^2$, where x_i is the fractional A-site occupancy of species i with radius r_i (Rodriguez–Martinez and Attfield 2001). A study of several series of manganates with fixed $\langle r_A \rangle$ and varying σ^2 shows that, as σ^2 is lowered, the phase-separated system transforms to a FM metallic state. It has been demonstrated recently that in a series of manganates of the type, $Ln_{0.7-x}Ln'_xA_{0.3-y}A'_yMnO_3$, where $\langle r_A \rangle$ always remains large (thereby avoiding effects due to bandwidth), a decrease in σ^2 transforms the insulating non-magnetic state to a FM metallic state (Kundu *et al* 2005). The most important evidence for electronic phase separation in manganates comes from direct observational evidence obtained from images employing transmission electron microscopy, scanning probe microscopy and photoemission microspectroscopy (Shenoy and Rao 2008). Such images clearly provide a convincing case for the presence of the electronic inhomogeneities.

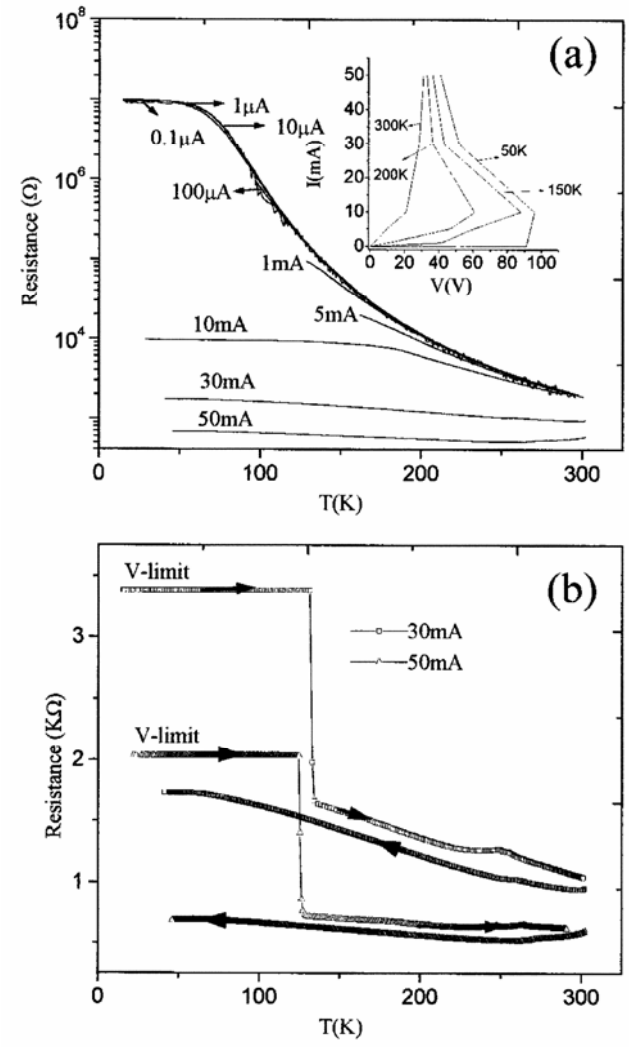

Figure 6. (**a**) Temperature variation of resistance of an oriented $Y_{0.5}Ca_{0.5}MnO_3$ film deposited on $LaAlO_3$ (100) for different values of the current and (**b**) resistance-temperature plots for two current values recorded over cooling and heating cycles showing memory effect. Inset in part a shows *I–V* curves at different temperatures (Rao *et al* 2000).

From the above discussion, it becomes clear that charge-ordered manganates generally show electronic phase separation. The origin of electronic phase separation itself must be somewhat chemical in nature. This view is substantiated by the effect of size mismatch of the A-site cations or phase separation. The coexistence of different phases requires that the strain energies of the domains at the boundaries should be comparable. Since the different domains would have different electronic properties they can give rise to large dielectric constants (Sudheendra and Rao 2003). Thus, the high dielectric constant of $CaCu_3Ti_4O_{12}$ is because of twin boundaries which may create a barrier layer capacitance (Subramanian *et al* 2000).

1.3 *Multiferroic nature of charge-ordered manganates*

It has been pointed out recently by Khomskii and coworkers (Efremov *et al* 2004) that coupling between magnetic and charge-ordering in charge-ordered and orbital-ordered perovskites can give rise to magnetoferroelectricity. As mentioned earlier, site-centred charge order (SCO) occurs around $x = 0{\cdot}5$ with a CE-type antiferromagnetic state while the bond-centred charge order (BCO) occurs around $x = 0{\cdot}4$ with a possible perpendicular spin structure. The composition with $x \sim 0{\cdot}45$ is predicted to have a ferroelectric ground state.

We have investigated the dielectric properties, magnetocapacitance and related features of rare earth manganates of the general formula, $Ln_{0.5}Ca_{0.5}MnO_3$ with Ln = Nd, Gd or Y, exhibiting short range charge-ordering (SCO). We have also examined the manganate compositions of the type, $Ln_{0.6}Ca_{0.4}MnO_3$, with Ln = Pr and Y, exhibiting BCO, which show canted antiferromagnetic or weak ferromagnetic behaviour at low temperatures due to electron phase separation (see figure 2b). They also show a broad maximum in the dielectric constant in the charge-ordering region and exhibit magnetocapacitance on the application of a magnetic field of 1 or 2 T. We shall now describe the results obtained with the $Y_{1-x}Ca_xMnO_3$ and $Pr_{0.6}Ca_{0.4}MnO_3$ compositions in some detail, since these manganates show the most robust charge-ordering.

2. Results and discussion

Nanoparticles of $Y_{0.5}Ca_{0.5}MnO_3$ and $Pr_{0.6}Ca_{0.4}MnO_3$ were prepared by the polymeric sol–gel method. The

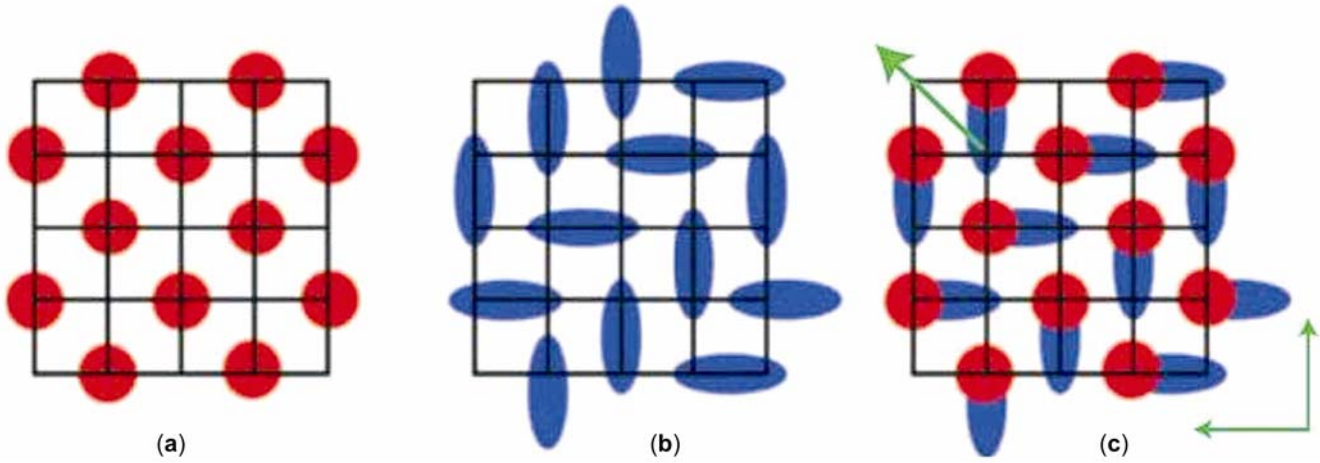

Figure 7. Three types of charge ordering: (**a**) site-centred charge order; (**b**) bond-centred charge order (the Zener polaron state); and (**c**) a ferroelectric intermediate state. The charge-ordered structure in *c* lacks inversion symmetry. Thin green arrows indicate the dipole moments of horizontal and vertical dimers, and the diagonal arrow is the total ferroelectric moment (Efremov *et al* 2004).

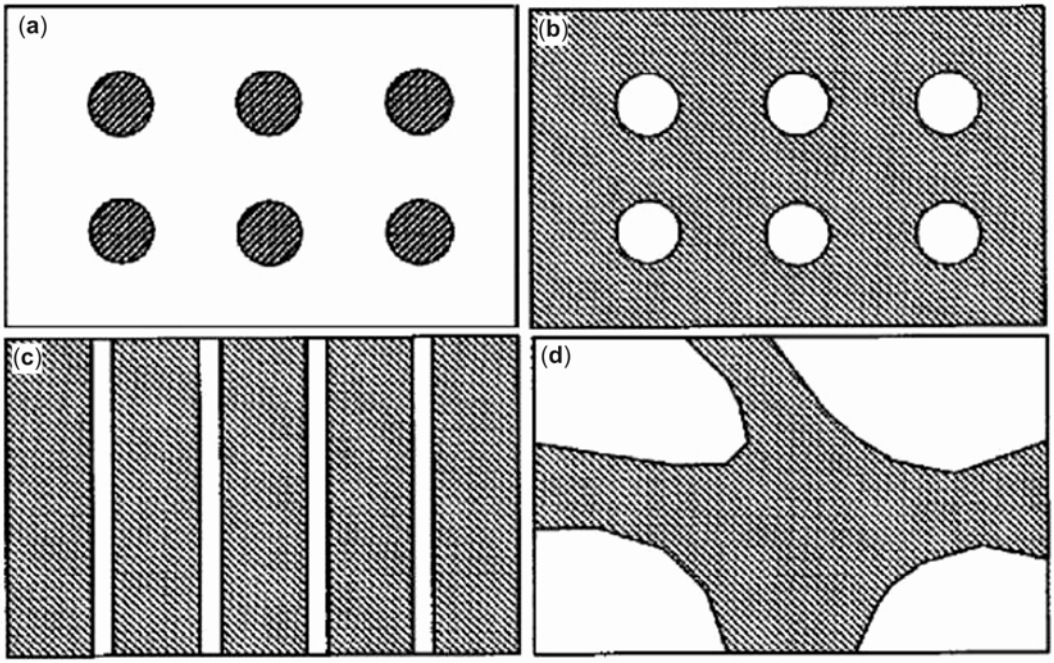

Figure 8. Schematic of electronic phase separation. Shaded portions indicate FM metallic regions; the unshaded portions correspond to AFM insulating regions. (**a**) FM metallic puddles in an insulating AFM background, (**b**) metallic regions with insulating droplets, (**c**) charged stripes and (**d**) phase separation on the mesoscopic scale.

nanoparticles with an average diameter of 30, 70 and 110 nm were prepared by heating at 600, 800 and 1000°C as evidenced from FESEM and TEM. The XRD patterns show greater broadening of the peaks in the samples prepared at lower temperatures.

The nanoparticles exhibit magnetic properties drastically different from the bulk samples prepared at high temperatures. The small particles do not show the charge-ordering transition or the antiferromagnetic transition. Instead, they show evidence for prominent ferromagnetic interaction, a feature that has been found in small particles of other charge-ordered rare earth manganates as well (Sudheendra *et al* 2002; Rao *et al* 2006; Zhang *et al* 2007). Our studies show that upon decreasing the particle sizes the ferromagnetic phase dominates over the antiferromagnetic phases. $Pr_{0.6}Ca_{0.4}MnO_3$ samples are much more ferromagnetic than the $Y_{0.5}Ca_{0.5}MnO_3$ samples because of the presence of the extra electron on the Mn^{+4}

sites which increase the ferromagnetic interaction in these samples.

$Y_{0.5}Ca_{0.5}MnO_3$ exhibits a charge-ordering transition at 275 K (T_{CO}) and an antiferromagnetic transition at 110 K (T_N) (Arulraj *et al* 1998). Ferromagnetic interactions are manifested at low temperatures due to electronic phase separation (Shenoy *et al* 2006; Shenoy and Rao 2008). Magnetic hysteresis is observed at $T < 20$ K, the values of remnant magnetization (M_r) and coercive field (H_C) at 5 K being 35 emu/mol and 489 Oe, respectively. In figure

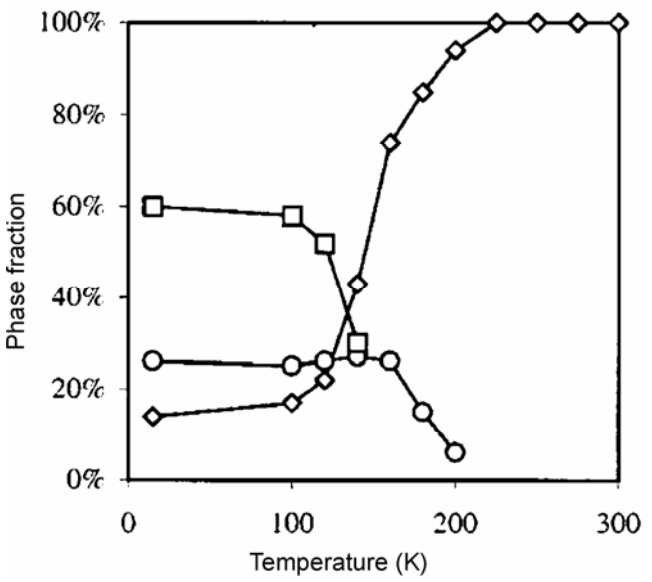

Figure 9. Variation in the percentage of the different phases of $Nd_{0.5}Sr_{0.5}MnO_3$ with temperature: FMM phase (diamonds); orbitally ordered *A*-type AFM phase (circles); charge-ordered CE-type AFM phase (squares) (Woodward *et al* 1999).

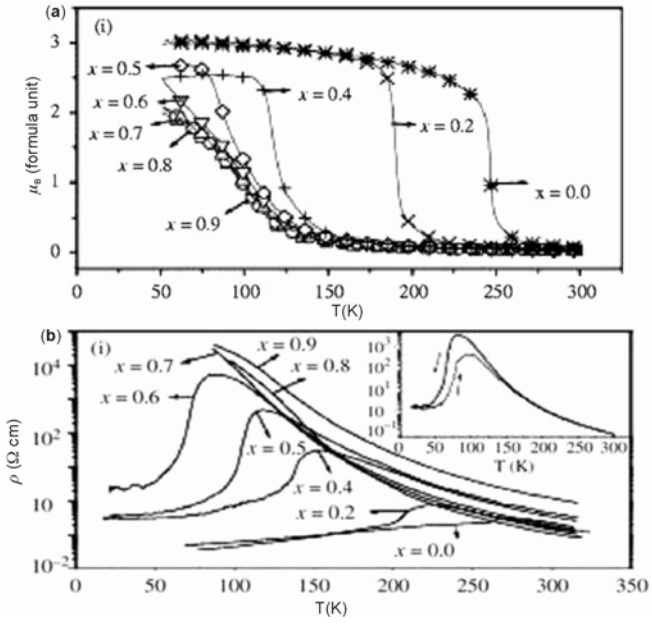

Figure 10. Temperature dependence of (**a**) the effective magnetic moment per formula unit and (**b**) the resistivity in $(La_{1-x}Nd_x)_{0.7}Ca_{0.3}MnO_3$. The insets show the 'resistivity hysteresis' upon warming of the sample (Sudheendra and Rao 2003).

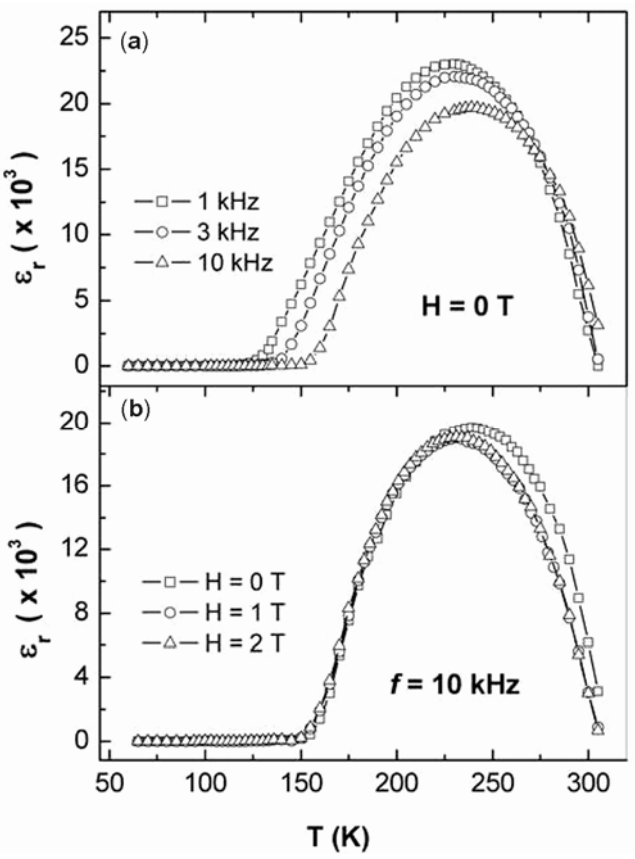

Figure 11. (**a**) Temperature-dependence of the dielectric constant of $Y_{0.5}Ca_{0.5}MnO_3$ at different frequencies and (**b**) effect of magnetic fields on the dielectric behaviour of $Y_{0.5}Ca_{0.5}MnO_3$ at 10 kHz.

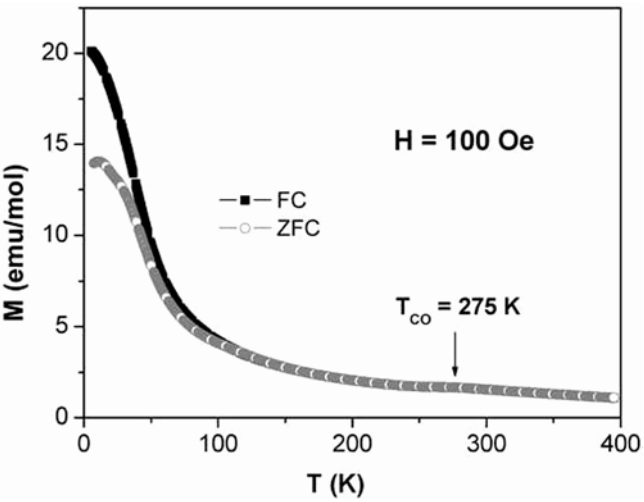

Figure 12. Variation of field-cooled (FC) and zero-field-cooled (ZFC) magnetizations of $Y_{0.55}Ca_{0.45}MnO_3$ as a function of temperature at a magnetic field of 100 Oe showing the charge-ordering transition at 275 K.

11(a), we have plotted the dielectric constant as a function of temperature for various frequencies. The dielectric constant exhibits a maximum in the 225–240 K range. On increasing the frequency, the dielectric constant decreases markedly with the maximum shifting to slightly higher temperatures. At 10 kHz, the maximum value of the dielectric constant is 2×10^4, which is high compared to other rare-earth manganates. This would be expected considering the robust charge-ordered state and small size of the yttrium ion. The ferroelectric transition temperature (T_{CE}) derived from the inverse Curie–Weiss plot of dielectric constant is close to T_{CO}. Application of a magnetic field of 1 T has a significant effect on the dielectric constant causing a shift of the dielectric constant maximum to a lower temperature as can be seen in figure 11(b).

Magnetic measurements on $Y_{0.55}Ca_{0.45}MnO_3$ show evidence for charge ordering at 275 K and weak ferromagnetic interactions below around 50 K (figure 12). It exhibits magnetic hysteresis loop at low temperatures, the values of M_r and H_C at 5 K being 45 emu/mol and 502 Oe, respectively. We show the temperature variation

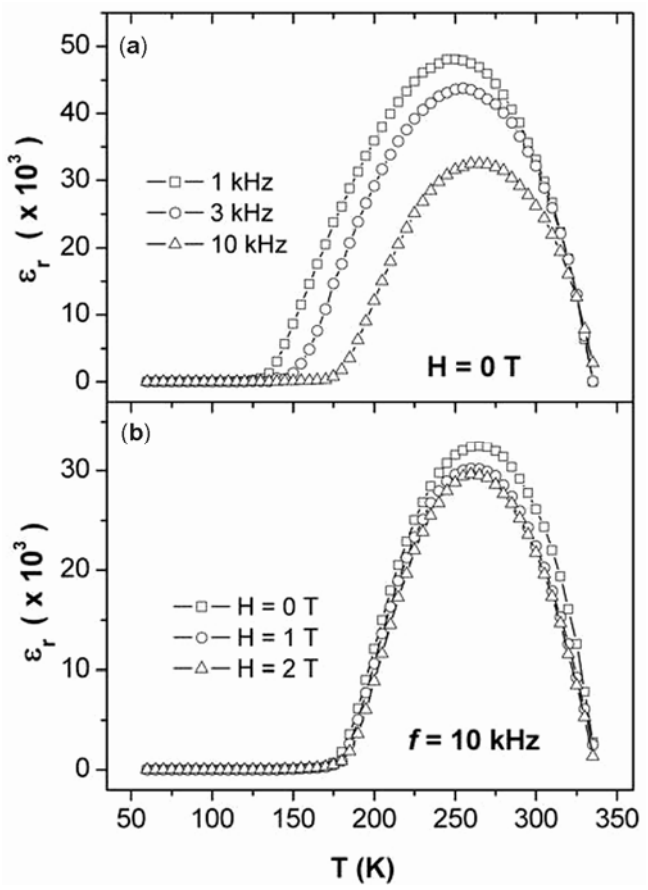

Figure 13. (**a**) Temperature-dependence of the dielectric constant of $Y_{0.55}Ca_{0.45}MnO_3$ at different frequencies and (**b**) effect of magnetic fields on the dielectric behaviour of $Y_{0.55}Ca_{0.45}MnO_3$ at 10 kHz.

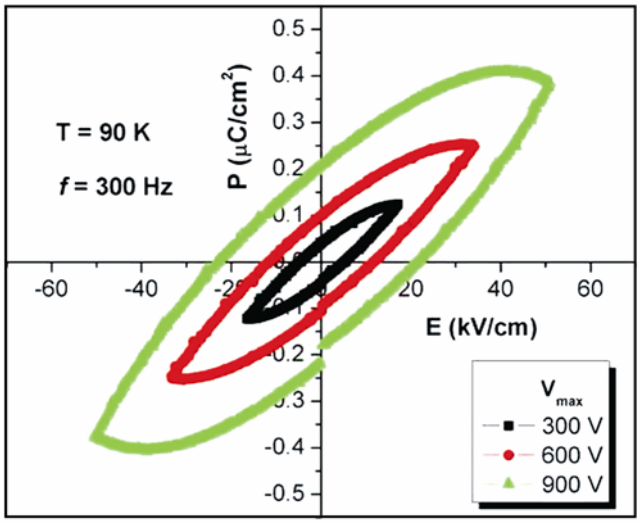

Figure 14. Ferroelectric hysteresis loops of a thin pellet of $Y_{0.55}Ca_{0.45}MnO_3$ (300 Hz) at 90 K for various voltages.

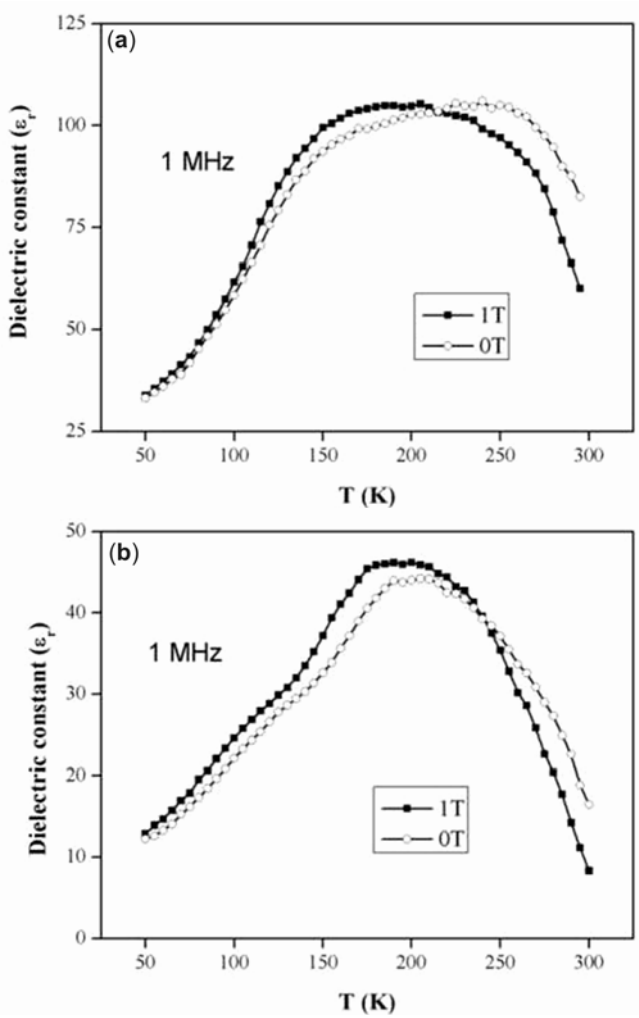

Figure 15. Effect of magnetic field on the temperature dependence of dielectric constant on nanoparticles of $Y_{0.5}Ca_{0.5}MnO_3$ prepared at (**a**) 600°C and (**b**) 800°C.

of the dielectric constant for $Y_{0.55}Ca_{0.45}MnO_3$ in figure 13(a). Based on the Curie–Weiss plot, we estimate T_{CE} to be 326 K which is much higher than that of $Y_{0.5}Ca_{0.5}MnO_3$. The maximum value of dielectric constant observed at 10 kHz is $3{\cdot}3 \times 10^4$. The effect of magnetic field on the dielectric constants is shown in figure 13(b). The data show clear evidence for magnetocapacitance. $Y_{0.6}Ca_{0.4}MnO_3$, with bond-centred charge ordering (BCO), also shows the properties similar to $Y_{0.5}Ca_{0.5}MnO_3$ with a T_{CE} of 300 K and magnetocapacitance at 1 *T*.

Since most of the rare-earth manganates possess relatively high conductivity, the dielectric hysteresis loops exhibited by them are similar to those of leaky dielectrics (Scott 2008). The dielectric hysteresis loop of a very thin sample (thickness, ~180 μm) of $Y_{0.55}Ca_{0.45}MnO_3$ (see figure 14) recorded by us shows a maximum polarization of around 0·43 μC/cm^2 and a remnant polarization of 0·25 μC/cm^2 at 900 V. In view of the possible unreliability of dielectric hysteresis loops (Scott 2008), we have examined second harmonic generation (SHG) by polycrystalline samples of $Y_{1-x}Ca_xMnO_3$ with $x = 0{\cdot}45$ and 0·4. The SHG responses of $Y_{0.55}Ca_{0.45}MnO_3$ and $Y_{0.6}Ca_{0.4}MnO_3$ were found to be 1·25 and 0·79 times that of quartz, respectively. These results establish that these charge-ordered manganates do indeed possess non-linear properties and polarization features of ferroelectrics.

In figures 15(a) and (b), we show the temperature variation of dielectric constant at 1 MHz with and without the application of the magnetic field (1*T*) for nanoparticles of $Y_{0.5}Ca_{0.5}MnO_3$ heated at 600 and 800°C, respectively. The dielectric constant of the $Y_{0.5}Ca_{0.5}MnO_3$ samples are much lower (by order of 1000) than the bulk samples. The magnetic field has a significant effect on the dielectric constant, the effect occurring over a wide temperature range of 75–300 K. Both the nano samples show positive magnetocapacitance below charge ordering transition temperature and negative after that as observed in the bulk samples.

In figures 16(a) and (b), we show the magnetocapacitive effect in $Pr_{0.6}Ca_{0.4}MnO_3$ at 1 MHz. The value of the dielectric constant is 3 orders less than the bulk samples (Serrao *et al* 2007; Sahu *et al* 2009). These samples also show a transition in broad temperature range. The nano samples prepared at 600°C show positive magnetocapacitance while those prepared at 800°C negative magnetocapacitance below 188 K and opposite after that. While the trend observed in the case of 600 sample is opposite to that of the bulk, the 800 samples show the same trend as the bulk.

3. Conclusions

Magnetocapacitance exhibited by these rare earth manganates is genuine since we do not observe any change in

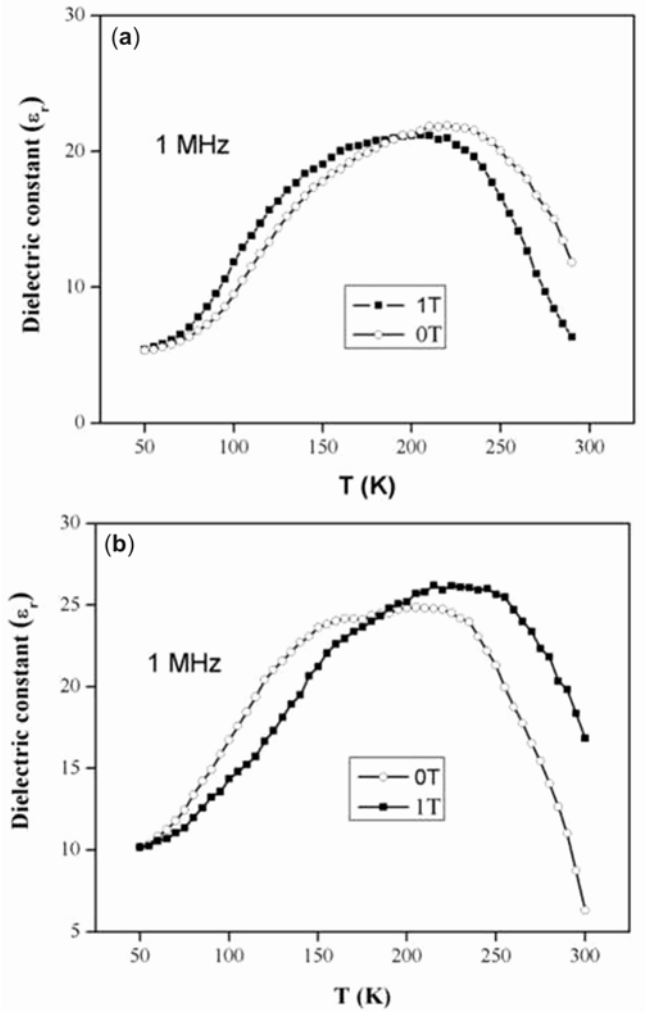

Figure 16. Effect of magnetic field on the temperature dependence of dielectric constant on nanoparticles of $Pr_{0.6}Ca_{0.4}MnO_3$ prepared at (**a**) 600°C and (**b**) 800°C.

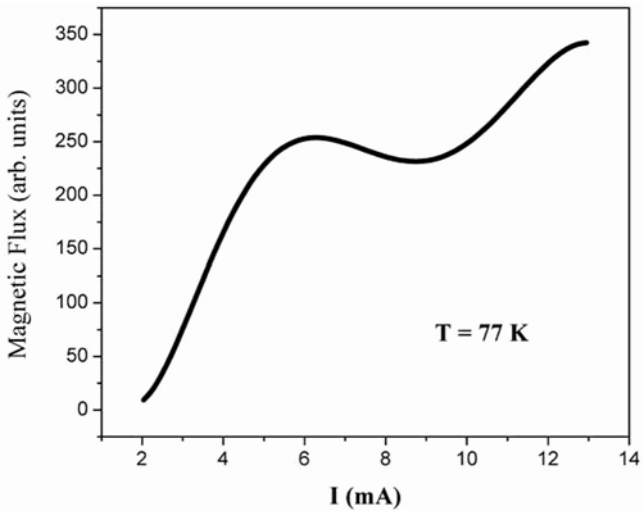

Figure 17. Magnetic flux (SQUID signal) at 77 K as a function of biasing current through the sample (Sudheendra *et al* 2002).

the resistance on the application of magnetic fields up to 7 *T* in the case of $Y_{1-x}Ca_xMnO_3$. Furthermore, these materials show a magnetic flux on the application of electric fields (Guha *et al* 2000; Sakai and Tokura 2008) (figure 17), indicating that there is interaction between the electric and magnetic order parameters. This would be expected since the metallic state created by the electric field should necessarily be ferromagnetic according to the DE mechanism. All these observations establish that the charge-ordered rare earth manganates, specifically the $Y_{1-x}Ca_xMnO_3$ compositions, are not only multiferroic but also magnetoelectric. These observations are consistent with the predictions of Efremov *et al* (2004). The magnetocapacitive behaviour of rare earth manganates may reflect the electronic phase-separation present in these materials wherein charge-ordered and ferromagnetic regimes or domains of different sizes coexist.

Acknowledgements

The authors thank Professor C N R Rao for suggesting the problem and guidance. One of us (JRS) thanks the University Grants Commission, Government of India, for a fellowship.

References

Arulraj A, Gundakaram R, Biswas A, Gayathri N, Raychaudhuri A K and Rao C N R 1998 *J. Phys.: Condens. Matter* **10** 4447

Cheong S W and Mostovoy M 2007 *Nat. Mater.* **6** 13

Dagotto E 2005 *Science* **309** 257

Eerenstein W, Mathur N D and Scott J F 2006 *Nature* **442** 759

Efremov D V, van den Brink J and Khomskii D I 2004 *Nat. Mater.* **3** 853

Guha A, Khare N, Raychaudhuri A K and Rao C N R 2000 *Phys. Rev.* **B62** R11941

Kimura T, Goto T, Shintani H, Ishizaka K, Arima T and Tokura Y 2003 *Nature* **426** 55

Kundu A K, Seikh M M, Ramesha K and Rao C N R 2005 *J. Phys.: Condens. Matter* **17** 4171

Kuwahara H, Tomioka Y, Asamitsu A, Moritomo Y and Tokura Y 1995 *Science* **270** 961

Lees M R, Barratt J, Balakrishnan G, Paul D McK and Yethiraj M 1995 *Phys. Rev.* **B52** R14303

Prellier W, Singh M P and Murugavel P 2005 *J. Phys.: Condens. Matter* **17** R803

Ramesh R and Spaldin N A 2007 *Nat. Mater.* **6** 21

Rao C N R 2000 *J. Phys. Chem.* **B104** 5877

Rao C N R and Raveau B (eds) 1998 *Colossal magnetoresistance, charge ordering and related properties of manganese oxides* (Singapore: World Scientific)

Rao C N R and Serrao C R 2007 *J. Mater. Chem.* **17** 4931

Rao C N R, Raju A R, Ponnambalam V, Parashar S and Kumar N 2000 *Phys. Rev.* **B61** 594

Rao S S, Tripathi S, Pandey D and Bhat S V 2006 *Phys. Rev.* **B74** 14416

Rodriguez-Martinez L M and Attfield J P 2001 *Phys. Rev.* **B63** 024424

Sahu J R, Serrao C R, Ghosh A, Sundaresan A and Rao C N R 2009 *Solid State Commun.* **149** 49

Sakai H and Tokura Y 2008 *Appl. Phys. Lett.* **92** 102514

Salamon M B and Jaime M 2001 *Rev. Mod. Phys.* **73** 583

Scott J F 2008 *J. Phys.: Condens. Matter* **20** 021001

Serrao C R, Sundaresan A and Rao C N R 2007 *J. Phys.: Condens. Matter* **19** 496217

Seshadri R and Hill N A 2001 *Chem. Mater.* **13** 2892

Shenoy V B and Rao C N R 2008 *Philos. Trans. R. Soc.* **A366** 63

Shenoy V B, Sarma D D and Rao C N R 2006 *Chem. Phys. Chem.* **7** 2053

Subramanian M A, Li D, Duan N, Reisner B A and Sleight A W 2000 *J. Solid State Chem.* **151** 323

Sudheendra L and Rao C N R 2003 *J. Phys.: Condens. Matter* **15** 3029

Sudheendra L, Chinh H D, Raju A R, Raychaudhuri A K and Rao C N R 2002 *Solid State Commun.* **122** 53

Tokura Y 2006 *Rep. Prog. Phys.* **69** 797

Tomioka Y, Asamitsu A, Kuwahara H, Moritomo Y and Tokura Y 1996 *Phys. Rev.* **B53** 1689

Van Aken B B, Palstra T T M, Filippetti A and Spaldin N A 2004 *Nat. Mater.* **3** 164

Vogt T, Cheetham A K, Mahendiran R, Raychaudhuri A K, Mahesh R and Rao C N R 1996 *Phys. Rev.* **B54** 15303

Wollan E O and Koehler W C 1955 *Phys. Rev.* **100** 545

Woodward P M, Vogt T, Cox D E, Arulraj A, Rao C N R, Karen P and Cheetham A K 1998 *Chem. Mater.* **10** 3652

Woodward P M, Cox D E, Vogt T, Rao C N R and Cheetham A K 1999 *Chem. Mater.* **11** 3528

Zhang T, Zhou T F, Qian T and Li X G 2007 *Phys. Rev.* **B76** 174415